



A Holocene temperature (brGDGT) record from Garba Guracha, a high-altitude lake in Ethiopia

Lucas Bittner¹, Cindy De Jonge², Graciela Gil-Romera^{3,4}, Henry F. Lamb^{5,6}, James M. Russell⁷, and Michael Zech¹

¹Heisenberg Chair of Physical Geography with focus on paleoenvironmental research, Institute of Geography, Technische Universität Dresden, Dresden, Germany

²Geological Institute, Department of Earth Sciences, ETH Swiss Federal Institute of Technology, 8092 Zurich, Switzerland

³Plant Ecology and Geobotany, Philipps University of Marburg, Marburg, Germany

⁴Department of Geoenvironmental Processes and Global Change, Pyrenean Institute of Ecology, CSIC, Zaragoza, Spain

⁵Department of Geography and Earth Sciences, Aberystwyth University, Aberystwyth, UK

⁶Department of Botany, School of Natural Sciences, Trinity College Dublin, Dublin 2, Ireland

⁷Department of Geological Sciences, Brown University, Providence, RI, USA

Correspondence: Lucas Bittner (lucas.bittner@tu-dresden.de)

Received: 12 April 2022 – Discussion started: 4 May 2022

Revised: 16 August 2022 – Accepted: 21 August 2022 – Published: 30 November 2022

Abstract. Eastern Africa has experienced strong climatic changes since the last deglaciation (15 000 years ago). The driving mechanisms and teleconnections of these spatially complex climate variations are yet not fully understood. Although previous studies on lake systems have enhanced our knowledge of Holocene precipitation variation in eastern Africa, relatively few studies have reconstructed the terrestrial temperature history of eastern Africa from lake archives. Here, we present (i) a new branched glycerol dialkyl glycerol tetraether (brGDGT) temperature calibration that includes Bale Mountains surface sediments and (ii) a quantitative record of mean annual air temperature (MAT) over the past 12 ka cal BP using brGDGTs in a sediment core collected from Garba Guracha (3950 m a.s.l.) in the Bale Mountains. After adding Bale Mountains surface sediment ($n = 11$) data (Baxter et al., 2019) to the existing East African lake dataset, additional variation in 6-methyl brGDGTs was observed, which necessitated modifying the MBT_{5ME} calibration (MBT denotes methylation of branched tetraethers) by adding 6-methyl brGDGT IIIa' (resulting in the MBT Bale Mountains index, $r^2 = 0.93$, $p < 0.05$). Comparing the MBT_{5ME} and the new MBT Bale Mountains index, our high-altitude Garba Guracha temperature record shows that warming occurred shortly after the Holocene onset when the temperature increased by more than 3.0 °C in less than 600 years. The highest temperatures prevailed between 9

and 6 ka cal BP, followed by a temperature decrease until 1.4 ka cal BP. The reconstructed temperature history is linked to supraregional climatic changes associated with insolation forcing and the African Humid Period (AHP), as well as with local anomalies associated with catchment deglaciation and hydrology.

1 Introduction

The severity of the current climate change and its global implications have been widely discussed following the latest report from the Intergovernmental Panel for Climate Change (IPCC) (IPCC, 2021). Uncertainty in future climate projection highlights the need for the scientific community to use palaeoclimate to estimate climate baseline conditions prior to human impact on climate (Neukom et al., 2019). Although palaeoclimatology has become a central discipline in understanding current climate variability (Thompson, 2004), important areas of the planet remain understudied. A partial understanding of global climate complexity can lead to biased views of natural systems (Hughes et al., 2021). This is the case for the African continent in general and north-eastern Africa in particular. Current climatic conditions in eastern Africa vary significantly due to its complex topography and the influence of the Intertropical Convergence Zone

(ITCZ), the Indian monsoon, and the El Niño–Southern Oscillation (ENSO). All of these affect temperature and the distribution, amount, and timing of rainfall in the region, resulting in a wide range of climatic conditions from the warm, dry, and semi-arid conditions of northern Kenya, southeastern Ethiopia, Djibouti, and Somalia to the cool, humid conditions of the western highlands (Hove et al., 2011; Nicholson, 2017; Lyon and Vigaud, 2017).

There is clear evidence indicating that, since the last glacial period, northern and eastern Africa have experienced severe climatic changes (Tierney et al., 2008, 2011b, 2017, 2013; Loomis et al., 2015; Wagner et al., 2018). Three major climate events are the post-glacial warming (~ 15 ka), the hydrological variability during the African Humid Period (AHP) (15–5 ka) (deMenocal et al., 2000) that led to the greening of the Sahara (Blom et al., 2009), and the drying period near the beginning of the Meghalayan (4.2 ka) (Bini et al., 2019). The intensity and the timing of these climatic changes varied regionally over northern and eastern Africa (Castañeda et al., 2016). While the driving mechanisms and the regional differences are complex and not fully understood, evidence supports the view that climatic changes in northern and eastern Africa were connected across the Northern Hemisphere (Tierney et al., 2013; Tierney and Russell, 2007; Otto-Bliesner et al., 2014). These complex teleconnections and their global impact support the importance of understanding long-term climate drivers in eastern Africa. Such knowledge will lead to better assessments of the impacts and potential mitigation of the current and future climate change scenarios in this world's understudied yet critical region.

While several studies have reconstructed the precipitation history in northern and eastern Africa over the last 15 ka cal BP (Bittner et al., 2021; Costa et al., 2014; Jaeschke et al., 2020; Junginger et al., 2014; Morrissey and Scholz, 2014; Tierney et al., 2011b; Trauth et al., 2018; Wagner et al., 2018), only a few have reconstructed the regional temperature history in northern and eastern Africa (Castañeda et al., 2016; Morrissey et al., 2018; Berke et al., 2012b; Loomis et al., 2017, 2012, 2015; Tierney et al., 2008, 2016). Moreover, there is a lack of terrestrial temperature reconstructions, especially in the high altitudes and the Horn of Africa. The Bale Mountains, situated in the east of the Rift Valley, are a valuable study site with the potential to enhance the palaeoclimatic knowledge in an understudied region.

For terrestrial archives, different methods have been developed and applied based on pollen, chironomids, and lipid biomarkers (Cheddadi et al., 1998; Wu et al., 2007; Chevalier and Chase, 2015; Bonnefille et al., 1992; Eggermont et al., 2010; Schouten et al., 2007). Over the last 15 years, an innovative approach for temperature reconstructions emerged based on branched glycerol dialkyl glycerol tetraethers (brGDGTs), membrane-spanning bacterial lipids (Damsté et al., 2000). Several calibration studies in different settings (i.e. soils and lakes) have shown a correlation between brGDGT abundances and mean annual air tempera-

ture (MAT) (e.g. De Jonge et al., 2014; Dearing Crampton-Flood et al., 2020; Russell et al., 2018; Weijers et al., 2007a). These calibrations have been successfully used to quantitatively reconstruct continental temperature in marine river outflow and lacustrine sediments and terrestrial archives such as loess sequences and palaeosoils (Loomis et al., 2015, 2017; Schreuder et al., 2016; Zeng and Yang, 2019; Garelick et al., 2022). Recently, global calibrations have been developed that suit cooler and more seasonal high-latitude lakes better (Martínez-Sosa et al., 2021; Raberg et al., 2021).

The phylogenetic breadth of the brGDGT-producing bacteria is still poorly constrained, although members from the phylum Acidobacteria have been proposed to produce brGDGTs both in cultures and in the environment (Sinninghe Damsté et al., 2018; De Jonge et al., 2019, 2021; Weber et al., 2018; van Bree et al., 2020). A recent study by Halamka et al. (2021) reports that Acidobacteria produce certain brGDGTs under oxygen limitation. Originally, Weijers et al. (2007b) found that the methylation of branched tetraethers (MBT) and cyclization of branched tetraethers (CBT) correlate with the measured mean annual air temperature (MAT) and pH values, respectively. Following the analytical separation of 5 and 6-methyl isomers, De Jonge et al. (2014) developed a new modified MBT'_{5ME} ratio. This resulted in a revised calibration that removed the pH dependence affecting the MBT and MAT correlation and improved the accuracy of MAT reconstructions in terrestrial and/or soil archives. As brGDGT distributions recovered from lake sediments showed a different MAT dependence compared to soils, Russell et al. (2018) developed an MBT'_{5ME} temperature calibration for lake sediments in eastern Africa. However, compared to the dataset of Russell et al. (2018), the brGDGT distribution of some Bale Mountains lake surface sediments are unique (Baxter et al., 2019). Although the MBT'_{5ME} calibration by Russell et al. (2018) is a valuable supraregional metric for reconstructing lake temperature, an adjusted calibration might better account for local conditions in the Bale region.

In this study, we aim to (i) compare brGDGT distributions from lake surface sediments of the Bale Mountains ($n = 11$) (Baxter et al., 2019) with the eastern African dataset (Russell et al., 2018), (ii) develop a new ratio that captures the unique variation in the Bale Mountains and compare the accuracy of this calibrated ratio with the MBT'_{5ME} , (iii) reconstruct the first Horn of Africa high-altitude palaeotemperature record in the Bale Mountains using the sedimentary record of Garba Guracha (3950 m a.s.l.), and (iv) compare this Garba Guracha temperature record with other records in the region.

2 Regional settings

2.1 Study area

Garba Guracha (6.875781° N, 39.878075° E; Fig. 1) and all other lakes in this study are located east of the Main Ethiopian Rift in the Bale Mountains of the Bale–Arsi Massif. More specifically, they are situated on the Sanetti Plateau, the highest plateau in the Bale Mountains, between ~ 3800 and ~ 4200 m a.s.l. with an area of 600 km² (Osmaston et al., 2005). Solidified horizontal lava consisting of tuffs with rhyolites, alkali basalt, and trachyte formed the volcanic plateau (Uhlig and Uhlig, 1991; Williams, 2016). The plateau and the valleys were partially glaciated at the Last Glacial Maximum (Groos et al., 2021a, b; Osmaston et al., 2005; Osendorf et al., 2019). The glacial cirque Garba Guracha was first mentioned by Werdecker (1962) and was also described in depth by Umer et al. (2007) and Tiercelin et al. (2008). With a maximum water depth of 6 m and a very small catchment area, the lake is located at 3950 m a.s.l. (0.15 km²; Fig. 1). The bedrock of the catchment is carbonate-poor (Löffler, 1978; Uhlig and Uhlig, 1991). An outlet towards the Togona Valley is present during the rainy season at the lake's northern end. A swampy alluvial plain fed by multiple springs stretches along the lake's southern shore.

2.2 Climate

The climate of the Bale Mountains varies spatially and temporally, affected by the orographic differences in altitude, a north–south exposure, and changing atmospheric air mass movements over the course of the year (Kidane et al., 2012; Uhlig and Uhlig, 1991). The Bale Mountains experience a 4-month dry season (November to February) and a long wet season with complex orographic rainfall patterns (March to October) (Woldu et al., 1989; Kidane et al., 2012). The complexity of the rainfall pattern is associated with the convergence of northeast and southwest winds due to the northern and southern location of the ITCZ between June and September and between October and March, respectively (Tiercelin et al., 2008; Kidane et al., 2012). The equatorial westerlies and the Indian Ocean monsoon act as two moisture sources for the precipitation in the Bale Mountains (Miehe and Miehe, 1994; Uhlig, 1988). With 1000–1500 mm yr⁻¹, the southern part of Bale Mountains experiences the highest precipitation amount, whereas the northern region, including Garba Guracha, only receives 800–1000 mm (Woldu et al., 1989). Temperatures vary seasonally, with the lowest temperatures in the dry season and the highest temperatures in the rainy season (Hillman, 1988). The Afroalpine regions, including the Sanetti Plateau, are characterized by diurnal temperature differences between day and night (–15 to +26 °C) (Hillman, 1988). Across the Bale Mountains, climate data have been collected since 2017 with a mean annual temperature of 4.9 °C (max 6, min 3.4 °C) at Angesso Station, located

at the same altitude 4 km northeast of Garba Guracha. The mean annual temperature at Garba Guracha is 5.4 °C (Baxter et al., 2019).

3 Material and methods

3.1 Material and sampling

In this study, we used the published data of 76 surface sediment samples from eastern African lakes. The data of these lakes, located mainly in Ethiopia, Uganda, and Kenya, were published by Loomis et al. (2014, 2011, 2012), Russell et al. (2018), Eggermont et al. (2011), and Baxter et al. (2019). The environmental data for the 11 lakes in the Bale Mountains were published by Eggermont et al. (2011) and Baxter et al. (2019), and the corresponding MAT is based on a calculated lapse rate supported by local climate station data (Loomis et al., 2012; Russell et al., 2018).

At the Garba Guracha site, two overlapping sediment cores were retrieved in February 2017, at a water depth of 4.8 m using a Livingstone piston corer. A maximum sediment depth of 1550 cm was reached, covering an organic-matter-rich upper section (0–900 cm) and an organic-matter-poor bottom one (900–1550 cm). This study focuses on the last 12.3 kcal BP covering the 0–950 cm, with a mean sedimentation rate of 15 yr cm⁻¹ (more details on sediment properties and chronology can be found in Bittner et al., 2020). We sampled at contiguous 10 cm intervals (average ~ 100 years of sedimentation). Thirty-five samples were selected for brGDGT analyses.

3.2 Sample preparation and analysis

The total lipid extract (TLE) of the surface sediment samples was extracted using an accelerated solvent extractor (ASE) with dichloromethane : methanol in a ratio of 9 : 1 (Loomis et al., 2012). The brGDGTs were purified and separated according to their polarity. The samples were quantified following the method described by Huguet et al. (2006).

The TLE of the downcore sediments was obtained using a Soxhlet system by constant rinsing (24 h) with solvent (dichloromethane : methanol in a ratio of 9 : 1). After rotary evaporation, the TLE was redissolved in *n*-hexane and transferred onto a pipette column filled with amino-propyl silica gel (Supelco, 45 µm). Solvents of increasing polarity (*n*-hexane, dichloromethane / methanol 2 : 1; diethyl ether/acetic acid 19 : 1) were used to selectively elute the fractions of the TLE (nonpolar fraction A; two polar fractions B and C, including brGDGTs). Fraction B contained 98 %–99 %, while fraction C contained 1 %–2 % of all brGDGTs. All results refer to the brGDGTs contained in fraction B. Before measurement, a C₄₆ brGDGT standard was added, and the extract was dried, redissolved in *n*-hexane / isopropanol (99 : 1), and filtered using a 0.45 µm polytetrafluoroethylene (PTFE) filter. The measurements of the GDGTs (dissolved

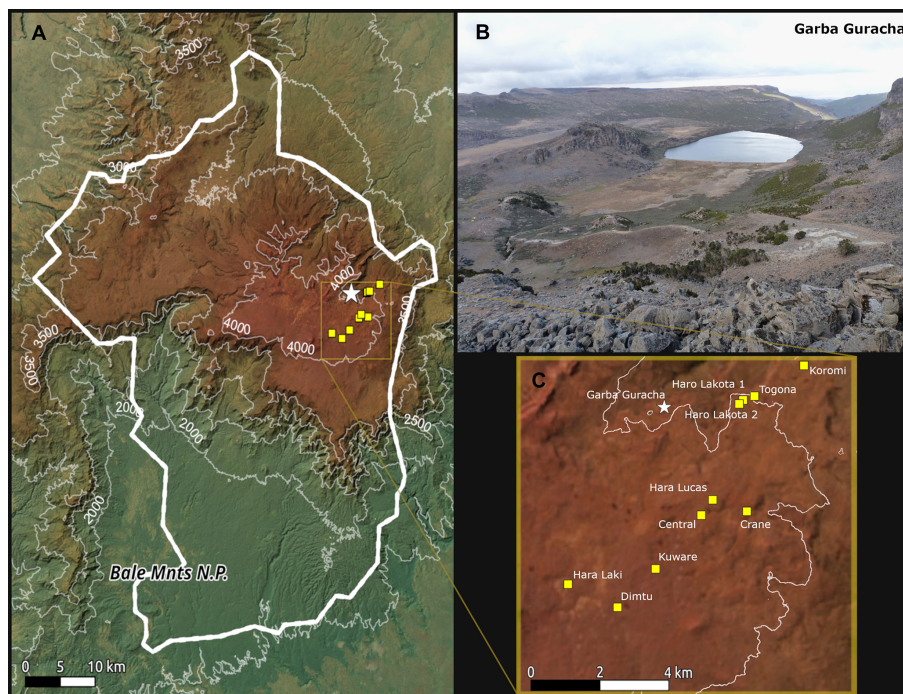


Figure 1. Location of the study area. (a) Bale Mountains National Park (thick white line); (b) a northeastward view over the glacial cirque of the Garba Guracha catchment (Bittner et al., 2021), and (c) Bale Mountains lakes in the dataset (yellow) – the map was created by the authors using QGIS 3.24 Tisler. All map layers are CC BY-SA v4.0; image is from Bing/DigitalGlobe © Microsoft; DEM is from NASA JPL SRTM (<http://www.jpl.nasa.gov/srtm/>, last access: 1 April 2022); the Bale Mountains National Park boundaries are from © OpenStreetMap contributors 2019. Distributed under the Open Data Commons Open Database License (ODbL) v1.0.

in *n*-hexane / IPA (99 : 1)) were made at ETH Zurich using a high-performance liquid chromatograph (Agilent 1260) coupled to a quadrupole mass spectrometer configured for atmospheric pressure chemical ionization (HPLC-APCI-MS). The separation of the GDGTs was achieved by two silica columns at 45 °C (modified after Hopmans et al., 2016) with a flow rate of 0.2 mL min⁻¹ and an injection volume of 10 µL. Compound-peak integrations of *m/z* 1292, 1050, 1048, 1046, 1034, 1032, 1022, 1020, 1018, and 744 were performed according to previously published methods (Hopmans et al., 2016).

3.3 BrGDGTs – structure, statistical methods, and proxy calculation

BrGDGTs can be present as tetramethylated (I), pentamethylated (II), or hexamethylated (III) compounds with different numbers of cyclopentyl moieties (none (a), one (b), or two (c)). The outer methyl group can be positioned on the α and/or ω C5 (5-methyl compounds) or C6 (6-methyl compounds), indicated by a prime notation (De Jonge et al., 2014). To interpret the GDGT composition of the samples, we used the branched and isoprenoid tetraether (BIT), MBT', MBT'_{SME}, and CBT' (Table 1).

We calculated the BIT index following the equation of Hopmans et al. (2004):

$$\text{BIT index} = \frac{\text{Ia} + \text{IIa} + \text{IIIa} + \text{IIa}' + \text{IIIa}'}{\text{Ia} + \text{IIa} + \text{IIIa} + \text{IIa}' + \text{IIIa}' + \text{crenarchaeol}} \quad (1)$$

De Jonge et al. (2014) showed that the MBT' ratio (Peterse et al., 2012) contains 5- and 6-methyl compounds that are explicitly mentioned here:

$$\text{MBT}' = \frac{\text{Ia} + \text{Ib} + \text{Ic}}{\left(\text{Ia} + \text{Ib} + \text{Ic} + \text{IIa} + \text{IIa}' + \text{IIb} + \text{IIb}' \right) + \text{IIc} + \text{IIc}' + \text{IIIa} + \text{IIIa}'} \quad (2)$$

By removing the 6-methyl isomers from the equation, De Jonge et al. (2014) improved the temperature calibration further:

$$\text{MBT}'_{\text{SME}} = \frac{\text{Ia} + \text{Ib} + \text{Ic}}{\text{Ia} + \text{Ib} + \text{Ic} + \text{IIa} + \text{IIb} + \text{IIc} + \text{IIIa}} \quad (3)$$

The cyclization of branched tetraethers (CBT') is calculated following the equation from De Jonge et al. (2014a):

$$\text{CBT}' = {}^{10} \log \frac{\text{Ic} + \text{IIa}' + \text{IIb}' + \text{IIc}' + \text{IIIa}' + \text{IIIb}' + \text{IIIc}'}{\text{Ia} + \text{IIa} + \text{IIIa}} \quad (4)$$

Russell et al. (2018) defined a calculation for surface water pH:

$$\text{surface water pH} = 8.95 + 2.65 \cdot \text{CBT}' \quad (5)$$

Lake water conductivity can be calculated using Eq. (12) of Raberg et al. (2021):

$$\begin{aligned} \ln(\text{conductivity}) = & 6.62 + 8.87 \cdot \frac{\text{Ib}}{\text{Ia} + \text{Ib} + \text{Ic}} \\ & + 5.12 \cdot \left(\frac{\text{IIa}'}{\text{IIa} + \text{IIb} + \text{IIc} + \text{IIa}' + \text{IIb}' + \text{IIc}'} \right)^2 \\ & + 10.64 \cdot \left(\frac{\text{IIa}}{\text{IIa} + \text{IIb} + \text{IIc} + \text{IIa}' + \text{IIb}' + \text{IIc}'} \right)^2 \\ & - 8.59 \cdot \frac{\text{IIa}}{\text{IIa} + \text{IIb} + \text{IIc} + \text{IIa}' + \text{IIb}' + \text{IIc}'} \\ & - 4.32 \cdot \left(\frac{\text{IIIa}'}{\text{IIIa} + \text{IIIb} + \text{IIIc} + \text{IIIa}' + \text{IIIb}' + \text{IIIc}'} \right)^2 \\ & - 5.31 \cdot \left(\frac{\text{IIIa}}{\text{IIIa} + \text{IIIb} + \text{IIIc} + \text{IIIa}' + \text{IIIb}' + \text{IIIc}'} \right)^2 \\ & - 142.67 \cdot \left(\frac{\text{IIIb}}{\text{IIIa} + \text{IIIb} + \text{IIIc} + \text{IIIa}' + \text{IIIb}' + \text{IIIc}'} \right)^2 \quad (6) \end{aligned}$$

The fractional abundance of any individual brGDGT compound (i) was defined as

$$f(i) = \frac{i}{\left(\text{Ia} + \text{Ib} + \text{Ic} + \text{IIa} + \text{IIa}' + \text{IIb} + \text{IIb}' + \text{IIc} + \text{IIc}' + \text{IIIa} + \text{IIIa}' + \text{IIIb} + \text{IIIb}' + \text{IIIc} + \text{IIIc}' \right)} \quad (7)$$

3.4 Quantitative data analyses

Numerical analyses in this paper have been performed with Excel and R 4.1.0 (R Core Team, 2021). Results are displayed using the arithmetic mean and standard deviations using the notation \pm . To explore the correlations between brGDGTs and MAT, we used linear regressions and the reported Pearson correlation values (r^2), where correlations were considered significant when the p value < 0.05 . We performed a principal component analysis (PCA) of brGDGTs from (i) the calibration dataset and (ii) the Garba Guracha record, based on standardized and scaled fractional abundance. The ordination methods provide a simple yet effective way to visualize the variability within the distribution of the brGDGTs. PCA was performed with the R package “factoextra” (Kassambara and Mundt, 2020).

4 Results

4.1 BrGDGT patterns of surface sediments from lakes in the Bale Mountains

To frame the downcore variation in Garba Guracha in the current environmental settings, we have expanded the dataset of

Russell et al. (2018) by 11 Bale Mountains lake surface sediment samples (Tables S1 and S2 in the Supplement) (data from Baxter et al., 2019). Due to the missing values of IIc, IIc', IIIb, IIIb', IIIc, and IIIc' in the paper by Russell et al. (2018), we excluded these isomers in the Bale Mountains data from the PCA to allow direct comparison of the PCAs (see Fig. S1 in the Supplement for different PCA including all isomers). The highest fractional abundances of brGDGTs in these surface sediments are (i) IIIa with a mean of 22 % (± 5 %), (ii) IIa with a mean of 22 % (± 7 %), and (iii) IIIa' with a mean of 16 % (± 12 %) (Fig. 2a and Table S2).

The PCA of brGDGTs shows some differences between the East African lake dataset and the Bale Mountains lakes (Fig. 2b). IIIa and IIa have negative loadings, and IIa', IIb', Ia, Ib, and Ic have positive loading on PC1. PC2 shows negative loadings from IIb and positive loading from IIIa' and IIa'. The Bale Mountains lakes have a negative score on PC1, consistent with their location in a cool climate. The similar distribution of tetra-, penta-, and hexamethylated brGDGTs in surface sediments illustrates a shared dominant lake-derived provenance with the East African lake dataset, as soil-derived brGDGTs are characterized by a larger fractional abundance of brGDGT Ia (Russell et al., 2018). At the same time, the Bale Mountains lakes have a wide dispersion on PC2, illustrating additional variation in brGDGTs. Regional differences in the brGDGT isomer abundances, especially in Bale Mountains surface sediments, are further supported by variations in the degree of cyclization (DC') and CBT' ratio values in the eastern African lake surface sediment data (Russell et al., 2018; Baxter et al., 2019) (Fig. S2). Specifically, on PC2, a decrease in IIb and an increase in IIIa' are visible in some of the Bale Mountains lakes, including Garba Guracha (highlighted in Fig. 2b).

Compared to similar high-altitude lakes (above 3500 m and MAT $< 10^\circ\text{C}$) in eastern Africa (Kenya and Uganda lakes previously published in the East African lake dataset; Russell et al., 2018), the percentage of IIIa and IIa is lower, and the percentage of IIIa' and IIa' is higher in the Bale Mountains lakes (Fig. 3). Interestingly, the combined percentage of these 5- and 6-methyl isomers is similar (Fig. 3a).

We hypothesize that the 6-methyl compounds (IIa' and IIIa') might be produced instead of their 5-methyl counterparts (IIa and IIIa), resulting in their higher fractional abundance in some of the Bale Mountains lakes (Fig. 3a). This is supported by our observation that, in the East African lake dataset, the correlation of %IIIa to MAT ($r^2 = 0.78$) is slightly improved by adding %IIIa' to $r^2 = 0.82$ (Fig. 3b and c). Narrowing the temperature range (MAT $< 10^\circ$), the improvement remains significant: the correlation of %IIIa to MAT ($r^2 = 0.11$; p value < 0.001) is improved by adding %IIIa' to $r^2 = 0.31$ (p value < 0.001) (Fig. S3). Although the production of IIIa' at the expense of IIIa is poorly understood in lacustrine settings, the isomerization of brGDGTs can be affected by the conductivity and salinity of the lake water (Raberg et al., 2021; Wang et al., 2021). As IIIa is a ma-

Table 1. Temperature calibrations – ratios, calibration dataset, r^2 , and root-mean-square error (RMSE) in degrees Celsius ($^{\circ}\text{C}$) – East African lake dataset (EAL), East African lakes + Bale Mountains lakes (EAL_{BM}).

Ratio	Calibration dataset	r^2	RMSE ($^{\circ}\text{C}$)
$\frac{\text{MBT}'_{5\text{ME}}}{\text{Ia}+\text{Ib}+\text{Ic}}$	EAL ($n = 65$)	0.92	2.41
$\frac{\text{Ia}+\text{Ib}+\text{Ic}}{\text{Ia}+\text{Ib}+\text{Ic}+\text{IIa}+\text{IIb}+\text{IIc}+\text{IIIa}}$	EAL _{BM} ($n = 76$)	0.92	2.41
$\frac{\text{MBT}'_{5\text{ME}} + \text{IIIa}'}{\text{Ia}+\text{Ib}+\text{Ic}+\text{IIa}+\text{IIb}+\text{IIc}+\text{IIIa}+\text{IIIa}'}$ (8)	EAL _{BM} ($n = 76$)	0.93	2.38
$\frac{\text{Simplified MBT}'_{5\text{ME}} + \text{IIa}' + \text{IIIa}'}{\text{Ia}+\text{IIa}+\text{IIIa}+\text{IIa}'+\text{IIIa}'}$ (9)	EAL _{BM} ($n = 76$)	0.84	3.48
$\frac{\text{Simplified MBT}'_{5\text{ME}} + \text{IIIa}'}{\text{Ia}+\text{IIa}+\text{IIIa}+\text{IIIa}'}$ (10)	EAL _{BM} ($n = 76$)	0.91	2.59

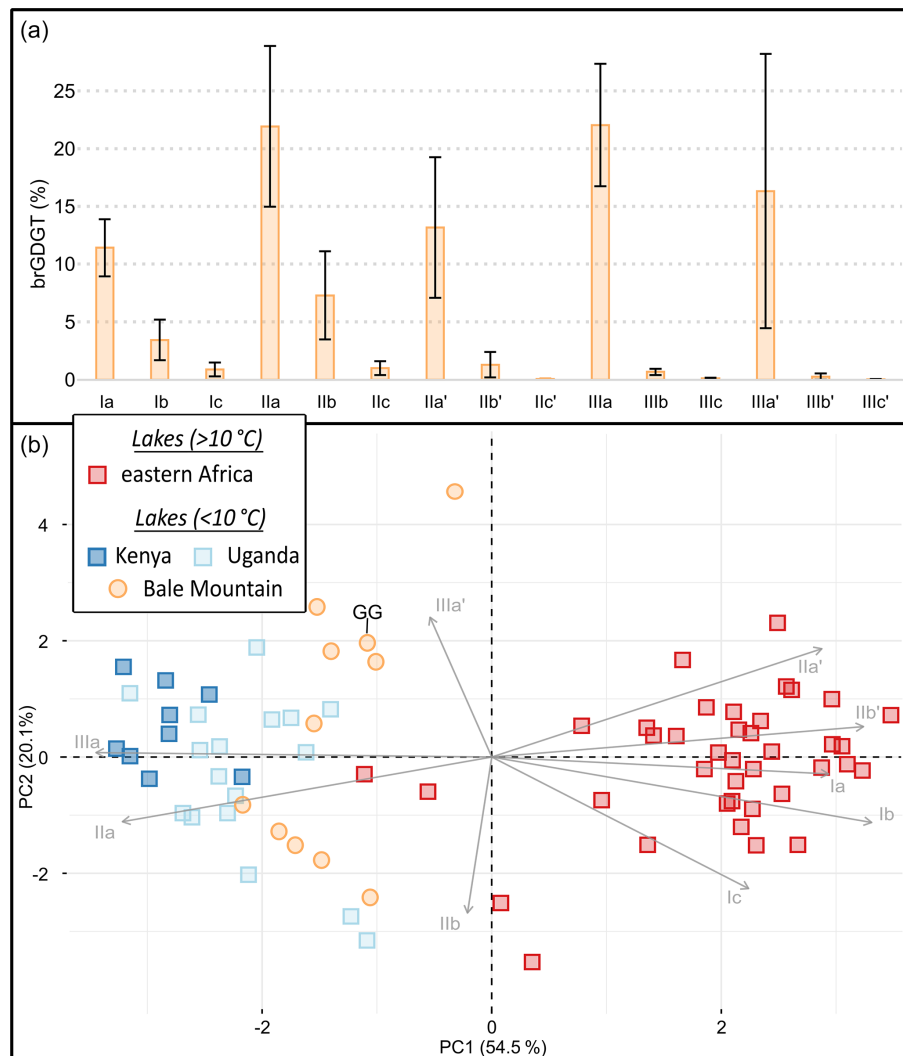


Figure 2. (a) Bar plot of average brGDGT percentages in Bale Mountains lake surface sediments (Baxter et al., 2019), with standard deviation plotted as error flags, and (b) PCA of brGDGTs of eastern African lakes with regional pattern; data from Russell et al. (2018) and Baxter et al. (2019) – lakes $> 10^{\circ}\text{C}$ (red) and lakes $< 10^{\circ}\text{C}$ (Bale Mountains – orange, Kenya – blue, and Uganda – light blue); Garba Guracha (GG).

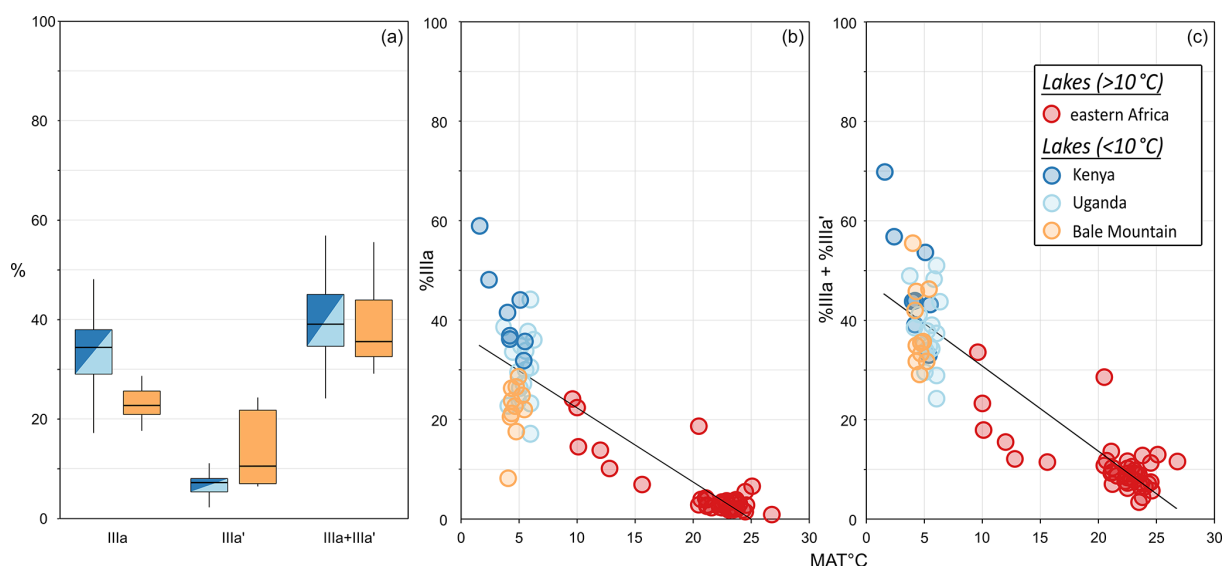


Figure 3. (a) Abundance (%) of IIIa and IIIa'; linear correlation between (b) IIIa (%) and MAT ($r^2 = 0.78$) and (c) IIIa + IIIa' (%) and MAT ($r^2 = 0.82$) – data from Russell et al. (2018) and Baxter et al. (2019) – lakes > 10 °C (red) and lakes < 10 °C (Bale Mountains – orange, Kenya – blue, and Uganda – light blue).

major component of the MBT'_{5ME} ratio, the hypothesized production of IIIa' at the expense of IIIa could have the potential to influence MBT'_{5ME} values. Indeed, MBT'_{5ME} values of the Bale Mountains lakes range from 0.20 to 0.37, with a mean of $0.24 (\pm 0.05)$. As the MAT range of Bale Mountains lakes is limited (4–5.4 °C), the range of MBT'_{5ME} is larger than expected of the measured MAT relative to similar eastern African lakes in the East African lake dataset ($MBT'_{5ME} = 0.17$ to 0.25 with a mean of 0.22 ± 0.02 ; MAT = 4 to 5.4 °C) (Russell et al., 2018).

4.2 BrGDGT patterns of the Garba Guracha sediment core

In general, the sediments of the Garba Guracha are characterized by a high input of aquatic organic matter. Several analysed proxies used to identify the source of organic matter indicate a predominantly aquatic production ($\delta^{13}C$, total organic carbon/nitrogen (TOC/N), P_{aq} , sugar quantification ratios) (Bittner et al., 2020, 2021). The composition of brGDGTs in the sediment of Lake Garba Guracha is inconsistent with the soil samples of Bale Mountains, indicating different producing communities (Fig. S4 and Table S3). These findings are concurrent with the results of Russell et al. (2018) that brGDGTs in eastern African lake sediments are dominantly lake-derived. Therefore, we suggest that most brGDGTs in the Garba Guracha sediment archive are also of aquatic origin.

In the Garba Guracha sediments, both branched and isoprenoid GDGTs are present. The BIT index ranges between 0.8 and 1 (mean = 0.98, ± 0.04). Only the oldest samples (12–10 kcal BP) have a lower BIT index value of 0.8

to 0.9 (Table S4). Tetramethylated brGDGTs in the sediment core represent on average 19.5 %, pentamethylated brGDGTs 44 %, and hexamethylated brGDGTs 36.5 % (Table S4). The highest fractional abundances are (i) IIIa with a mean of 21 % (± 5 %), (ii) Iia with a mean of 20 % (± 3 %), and (iii) Ia with a mean of 15 % (± 3 %). The MBT'_{5ME} ranges from 0.20 to 0.35 with a mean of $0.28 (\pm 0.04)$ (Table S5). The CBT' ratio ranges from 0.06 to -0.54 with a mean of $0.27 (\pm 0.18)$ (Table S4).

A PCA of all downcore brGDGTs distributions (Fig. 4a) shows that the first two components explain 63.2 % of the variance. On PC1 (42.3 %), all 6-methyl isomers have negative loadings, while 5-methyl isomers show positive loadings. PC2 (20.9 %) shows positive loadings of all hexamethylated brGDGTs and negative loadings of all penta- and tetramethylated brGDGTs. The PCA reveals changes in brGDGT composition with core depth when the data points are grouped using the following age cut-offs: 0–4.3, 4.3–10.5, and 10.5–12.5 kcal BP (Fig. 4a). In phase 1 (12.5–10.5 kcal BP), IIIa, IIIa', and Iia have the highest mean abundances of 30 %, 17 %, and 17 %, respectively. In phase 2 (10.5–4.3 kcal BP), the mean abundances of IIIa and IIIa' are decreased by around 9 %, while Iia, Iib, and Ia increase. In phase 3 (4.3–0 kcal BP), the mean abundances of IIIa decrease by 6 % further. Conversely, the mean abundance of IIIa' increases again by 12 %. The same holds true for Iia (–5 %) and Iia' (+6 %). The mean abundance of Ia increases further by 3 % (Fig. 4b).

The unusually high abundance of brGDGTs IIIa' compared to IIIa observed in surface sediments of Bale Mountains lakes (Fig. 2a) is also visible in the Garba Guracha record, and the relative abundance of IIIa' varies with depth.

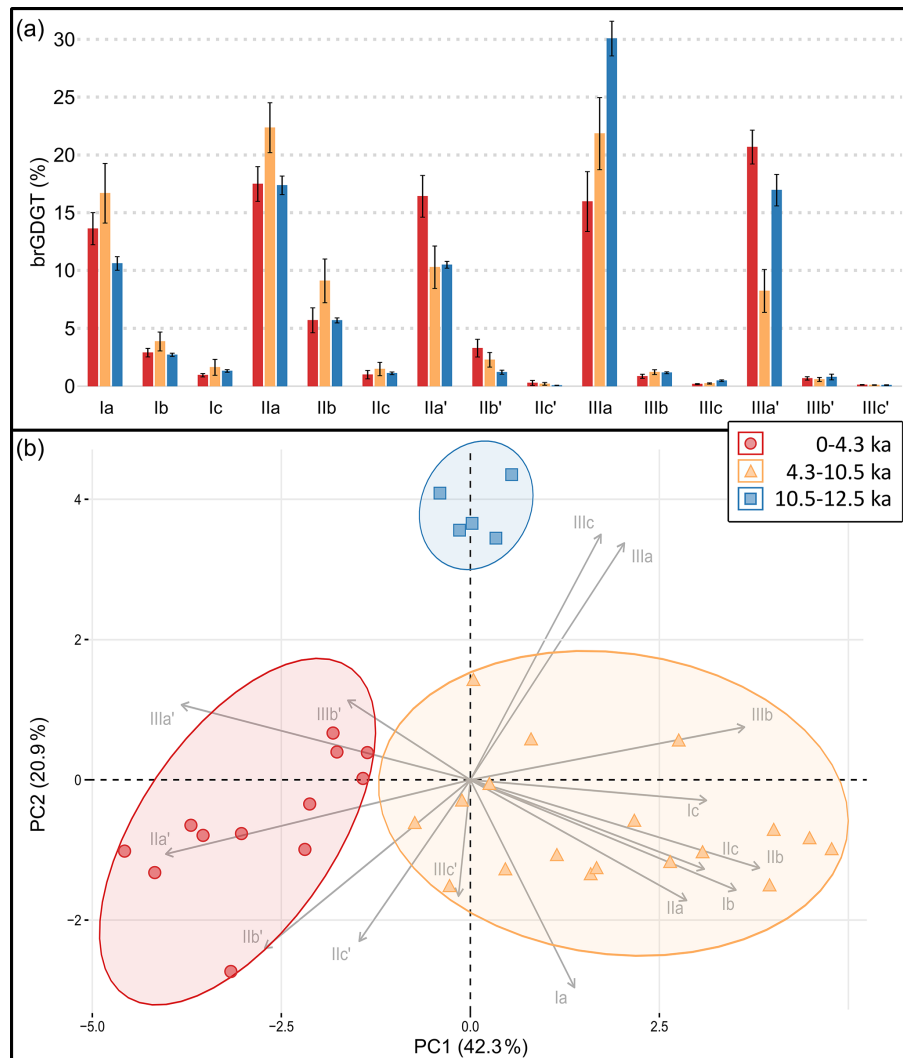


Figure 4. (a) Bar plot of average brGDGT percentages in the Garba Guracha sediment core, with standard deviation plotted as error flags; (b) PCA of brGDGTs of the Garba Guracha sediment core; data from 0 to 4.3 ka BP (red), 4.3 to 10.5 ka BP (orange), and 10.5 to 12.5 ka BP (blue).

High amounts of IIIa' appear until 10.8 ka BP followed by a low percentage ($< 10\%$) until 4.5 ka BP. The highest abundance of IIIa' with up to 22% occurs after 4.5 ka BP until the recent past. The changing abundances of IIIa' in our record coincide with changes in CBT' (Fig. 5). The variability in the 6-methyl brGDGTs reflects the largest part of the variation in this dataset, reflected by the good agreement ($r^2 = 0.77$, $p < 0.001$) between the fractional abundance of brGDGTs IIIa' and the sample loadings on PC1.

5 Discussion

5.1 Possible MAT calibration functions inferred from the expanded eastern African surface sediment dataset

We added the GDGT distribution data of 11 surface sediments from Bale Mountains lakes (Baxter et al., 2019) to the existing data of Russell et al. (2018) and applied the MBT'_{5ME} calibration (Table 1). Here, the original dataset ($n = 65$) is referred to as East African lakes “EAL”, while the extended dataset ($n = 76$) is referred to as East African lakes + Bale Mountains lakes (EAL_{BM}). The linear correlation between the MBT'_{5ME} and MAT was almost identical after adding the 11 Bale Mountains lake samples (EAL $r^2 = 0.92$, EAL_{BM} $r^2 = 0.92$). In the tropical Bale Moun-

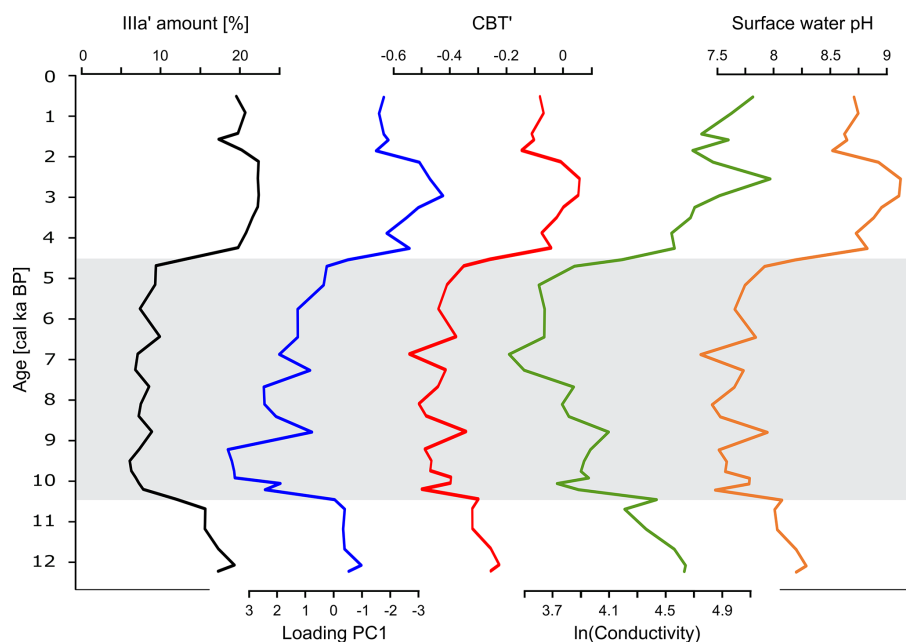


Figure 5. Downcore functions for IIIa' amount, the PC1 loading, CBT', ln(conductivity) (Eq. 12 in Raberg et al., 2021), and surface water pH of the Garba Guracha brGDGT record.

tains, the freezing of lakes is extremely rare, due in part to the intense year-round insolation, and MAT is equal to the average air temperature of months above freezing (MAF). To test whether the unique brGDGT distribution in some Bale Mountains lakes (Fig. 2) affected the temperature correlation, we applied various calibrations to account for the increased abundance of IIIa' (and to a lesser extent IIa'). In the EAL_{BM} dataset, the application of this ratio has a lower r^2 of 0.84 and a higher RMSE of 3.48 °C compared to the MBT'_{5ME} (Table 1, Eq. 9). As brGDGT IIIa' specifically was shown to increase in Bale Mountains sediments and improved the correlation with MAT (Fig. 3b and c), we investigated alternative ratios that incorporate this compound but exclude IIa'. Table 1 and Fig. 6 summarize the correlation coefficients of the MBT'_{5ME} ($r^2 = 0.92$, RMSE of 2.41 °C), an MBT'_{5ME} ratio that includes IIIa' (Eq. 10) with $r^2 = 0.93$ and RMSE of 2.38 °C, and the simplified ratio that includes only the major brGDGTs compounds (Eq. 10, $r^2 = 0.91$ and an RMSE of 2.59 °C).

The results of the calibrations $Ia/(Ia + IIa + IIIa + IIIa')$ ($MAT = -0.773 + 35.646 \cdot Ia/(Ia + IIa + IIIa + IIIa')$) and $MBT'_{5ME} + IIIa'$ ($MAT = -1.4734 + 35.777 \cdot MBT'_{5ME} + IIIa'$) applied to the Garba Guracha sediment core are very similar and correlate well ($r^2 = 0.97$) (Fig. 7, purple and turquoise curves, respectively). Therefore, we will only discuss the best-performing calibrations developed using the EAL_{BM} dataset MBT'_{5ME} ($MAT = -1.8299 + 33.304 \cdot MBT'_{5ME}$) and the MBT'_{5ME} + IIIa' calibration to the downcore distributions.

5.2 Palaeotemperature reconstructions for the Garba Guracha sedimentary record – comparison of the different calibrations

We evaluate the downcore trend in GG sediments to compare the performance of both calibrations, revealing periods of agreement (10–4.2 ka) and a period of temperature offset (since 4.2 ka). Using established and newly developed ratios and calibrations ($MBT'_{5ME} + IIIa'$ and MBT'_{5ME} EAL_{BM}) resulted in similar absolute values and comparable temperature trends, principally in the Early Holocene and Mid-Holocene. Reconstructed temperatures range from 4.9 to 10.0 °C (MBT'_{5ME}) and 4.2 to 9.5 °C ($MBT'_{5ME} + IIIa'$) (Fig. 7). Despite a slightly different range in temperature (4.4 and 5.3 °C), the trends of both calibrations are similar between 12 and 4.7 ka cal BP. The lowest MATs (< 5 °C) occurred between 12.2 ka cal BP (950 cm) and 10.5 ka cal BP (800 cm). MAT increased rapidly by 3.5 °C between 10.5 ka cal BP (800 cm) and ca. 10 ka cal BP (700 cm). During the Early Holocene to Mid-Holocene, a thermal maximum occurred between 10 and 5.7 ka cal BP (440 cm), with the highest MAT values reaching ca. 10 °C. At ~ 6.5 ka cal BP, the MAT decreased for both calibrations. The temperature drop coincides with organic-poor layers in the sediment core formed during a drought, associated with low monsoonal intensity (Bittner et al., 2020). A strong offset between the calibrations appeared at 4.2 ka cal BP, at a moment when temperatures are expected to decrease in phase with insolation (Fig. 7). Using the MBT'_{5ME}, we reconstruct a sudden temperature rise (Fig. 7) that contrasts with the temperature decrease when

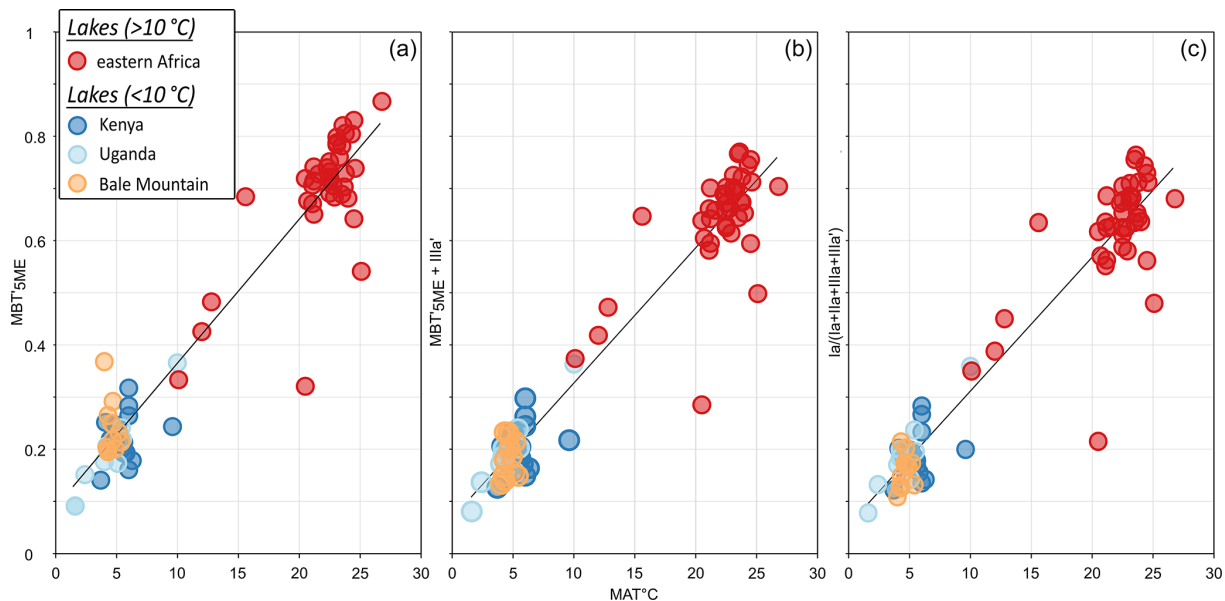


Figure 6. Correlations of EAL_{BM} datasets: (a) MBT'_{5ME} ($r^2 = 0.92$; RMSE of 2.41); (b) $MBT'_{5ME} + IIIa'$ ($r^2 = 0.93$; RMSE of 2.38); (c) $Ia/(Ia + IIa + IIIa + IIIa')$ ($r^2 = 0.91$; RMSE of 2.59) – data from Russell et al. (2018) and Baxter et al. (2019) – lakes $> 10^\circ\text{C}$ (red) and lakes $< 10^\circ\text{C}$ (Bale Mountains – yellow, Kenya – blue, and Uganda – light blue).

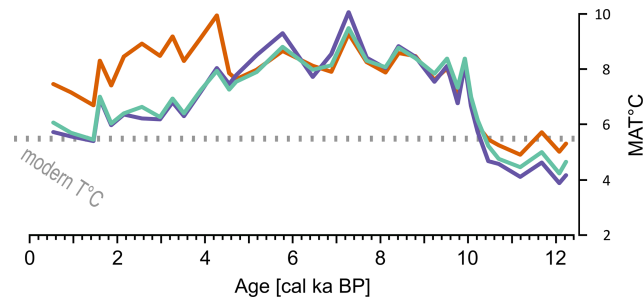


Figure 7. Reconstructed temperatures of the Garba Guracha sedimentary record. MBT'_{5ME} (orange); $Ia/(Ia + IIa + IIIa + IIIa')$ (purple); $MBT'_{5ME} + IIIa'$ (turquoise).

using the $MBT'_{5ME} + IIIa'$ calibration. The offset coincides with a known drought phase and is accompanied by shifts in many proxies (TOC, $\delta^{13}\text{C}$, TOC/N, *Erica* spp., charcoal) in the Garba Guracha sediments (Bittner et al., 2020; Gil-Romera et al., 2019). The changing conditions in the Garba Guracha catchment during this drought phase, especially the decline of the *Erica* shrubland (Gil-Romera et al., 2019), might have increased the surface water pH (Fig. 5). A change in the lake water chemistry is supported by changes in the reconstructed surface water pH (7.3–9.1) and conductivity (30–189; reported in Fig. 5 as $\ln(\text{conductivity})$) of the lake water (Fig. 5; calibrations from Russell et al., 2018, and Raberg et al., 2021). In the last few years, studies have suggested that the change in brGDGT composition captured by the CBT' may change due to shifting bacterial communities

in soils and lakes (De Jonge et al., 2019; van Bree et al., 2020; Weber et al., 2018). Previously, pH, conductivity, and salinity-dependent brGDGTs composition, sometimes driven by community changes, have been shown to affect MBT'_{5ME} values in soils and lake sediments (De Jonge et al., 2021; Wang et al., 2021; Raberg et al., 2021), and we propose that a similar effect can be seen in Garba Guracha.

Hence we suggest that MBT'_{5ME} systematically overestimates the temperatures of Garba Guracha during the Late Holocene after 4 kcal BP. A systematic offset is further supported by continuously and similarly decreasing reconstructed temperatures using both calibrations until the top of the core with a shared maximum at 150 cm (1.6 kcal BP). We suggest that the production of $IIIa'$ at the expense of $IIIa$ is increased during drier intervals, possibly caused by a change in lake water chemistry and/or bacterial communities. We conclude that a temperature calibration including $IIIa'$ allows us to reconstruct MAT in Garba Guracha sediments more accurately as it accounts for the unique and variable production of $IIIa'$ in Bale Mountains lakes.

5.3 Palaeotemperature reconstructions for the Garba Guracha sedimentary record – regional comparison

In contrast to precipitation reconstructions based on $\delta^2\text{H}$ in East Africa (Garelick et al., 2021), the temperature records do not show a clear meridional, north–south temperature change or an east–west pattern. The reconstructed overall temperature ranges are, however, consistent with the elevations of the lake archives. The amplitude of temperature

change over the last 13 kyr at Garba Guracha is $\sim 6^{\circ}\text{C}$. Similar amplitudes of change have been reconstructed at other high-altitude sites (Lake Mahoma and Lake Rutundu) (Loomis et al., 2017; Garelick et al., 2022), whereas equatorial records at lower elevations yield lower temperature amplitudes (Lake Victoria and Lake Tanganyika) (Tierney et al., 2008; Berke et al., 2012b), and higher temperature amplitudes are also recorded in the northeast African Lake Tana (Loomis et al., 2015). In fact, Garba Guracha has some of the highest-amplitude temperature changes of all of the sites during the Holocene, perhaps because it combines high elevation with a slightly higher latitude than other terrestrial African temperature records.

5.3.1 Deglacial warming

Overall, the recorded temperature trends in Garba Guracha are in phase with northern summer insolation variability (Fig. 8). This is reasonable because air temperature and insolation are closely connected (Huybers, 2006). However, the coldest MATs ($< 5^{\circ}\text{C}$) were recorded before 10.5 ka cal BP even though the Northern Hemisphere summer (20°N) insolation maxima had occurred already at 12 ka cal BP (Fig. 8). Tiercelin et al. (2008) argue that in Garba Guracha, ice remained in the catchment until ~ 10 ka cal BP due to topographical conditions, especially the north-facing exposition of the valley. The remaining ice in the basin might have (i) reduced the temperature of the lake water by inflow of cold meltwater and (ii) buffered the air temperature warming caused by increasing insolation. Indeed, rising temperatures were recorded in other eastern African records as early as 21 ka cal BP (Lake Mahoma) (Garelick et al., 2022) and in Ethiopia as early as 14 ka cal BP (Lake Tana) (Loomis et al., 2015; Tierney et al., 2016).

Similarly to Lake Tana but ~ 4000 years later, MAT ($^{\circ}\text{C}$) in the Garba Guracha record experienced an abrupt increase of ca. 3.5°C in just ca. 600 years, from 10.5 to 9.9 ka cal BP. Simultaneously with the rise in temperature, Bittner et al. (2021) found an increase in the precipitation/evaporation ratio (P/E), indicating higher moisture availability based on depleting values of reconstructed $\delta^{18}\text{O}_{\text{lake water}}$. At Lake Tana, Loomis et al. (2015) and Costa et al. (2014) attribute a similar connection between warmer temperature and depleted water isotopes ($\delta^2\text{H}$) since 13.8 ka cal BP to the penetration of warm Congo Basin air masses resulting in weaker easterly trade winds and a strengthening of the southwesterly winds and the Somali jet. The connection between Congo Basin air masses and eastern Africa is supported by the absence of cold temperatures associated with the Younger Dryas (YD) in both the Congo Basin temperature record (Weijers et al., 2007a) and Lake Tana (Loomis et al., 2015). However, in the Garba Guracha record, lower temperatures prevailed for 4000 years longer than in Lake Tana (Loomis et al., 2015). Although catchment glaciers could have caused these conditions in Garba Guracha, the low temperatures are

accompanied by a reduced sedimentation rate between 12.8 and 11.3 ka cal BP (Bittner et al., 2020), pointing to climatic influences associated with YD times (Alley, 2000). Indeed, other records from the Horn of Africa indicate dry conditions associated with the YD period, like Lake Ashenge (Marshall et al., 2009), and the marine record of the Gulf of Aden (Tierney and deMenocal, 2013). Therefore, we suggest that, at least for some periods, the climate drivers operating in the Garba Guracha region might have been different from other parts of eastern Africa. The time lag between Lake Tana and Garba Guracha could be explained by a slow eastward advance of the Congo Air Boundary and different climatic conditions at the sites. However, with the current data, we are unable to precisely distinguish between Northern Hemisphere YD forcing, remaining ice in the lake catchment, and regional atmospheric circulation change affecting the Garba Guracha record.

5.3.2 Warm temperatures during the African Humid Period in eastern Africa

Regardless of the cause, the ~ 10.5 ka cal BP rise in MAT is associated with abrupt increasing moisture availability and changes in vegetation around Garba Guracha (Gil-Romera et al., 2021; Umer et al., 2007). Vegetation and fire dynamics around Garba Guracha responded dynamically to the changing climatic conditions, evidencing the sensitivity of the Afroalpine–Afroalpine plant communities to increasing temperature. As MAT increased between 11 and 10 ka cal BP, the ericaceous belt expanded (Gil-Romera et al., 2021). The rising temperature and increasing P/E (Bittner et al., 2021) were accompanied by the expansion of the Afroalpine vegetation cover (Gil-Romera et al., 2021; Miehe and Miehe, 1994). An immediate consequence of the temperature rise and increasing moisture availability was biomass accumulation, as evidenced by the change from organic-matter-poor to organic-matter-rich sedimentation (Bittner et al., 2020) and the expansion of heathlands (Gil-Romera et al., 2019). Under an increasing MAT and extending biomass, fire activity was very intense at this time (Gil-Romera et al., 2019).

The thermal maximum of the Garba Guracha record spanned from 9 to 5.8 ka cal BP, with the highest reconstructed temperatures occurring at 7 ka cal BP. A similar Mid-Holocene thermal optimum has been recorded at Sacred Lake (7 ka cal BP) and Lake Tana (7 ka cal BP) (Fig. 8). However, the highest temperatures of Lake Victoria occurred at 9 ka cal BP and of Lake Rutundu, Lake Malawi, and Lake Tanganyika at 5 ka cal BP (Berke et al., 2012a; Loomis et al., 2017, 2015, 2012; Powers et al., 2005; Tierney et al., 2008; Garelick et al., 2022). At Lake Turkana, the thermal optimum occurred at 6.4 ka cal BP (Morrissey et al., 2018) or 5 ka cal BP (Berke et al., 2012b). A new temperature reconstruction from Lake Mahoma (Garelick et al., 2022) and a temperature stack including temperature reconstructions from Sacred Lake, Lake Malawi, Lake Tanganyika,

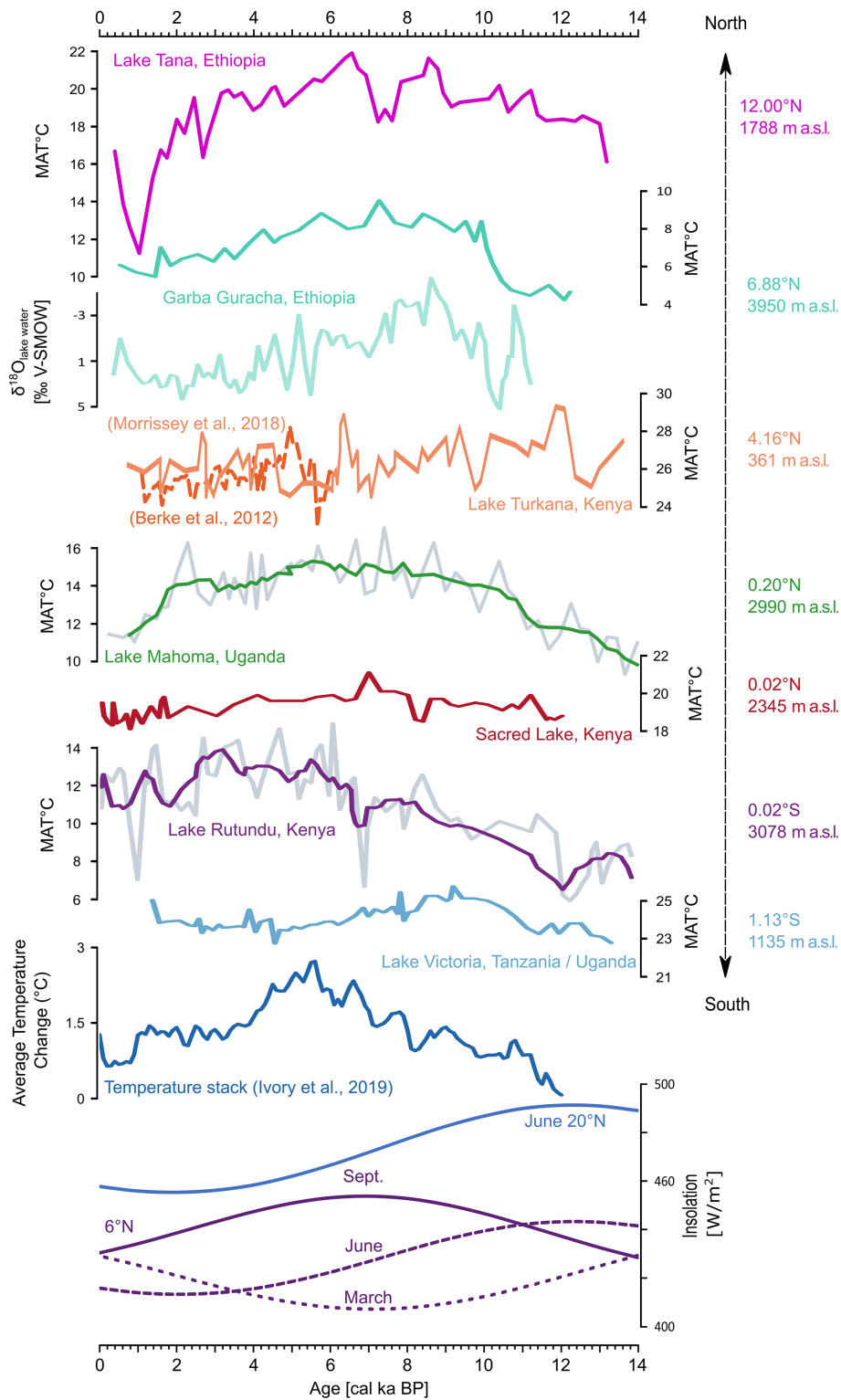


Figure 8. Comparison of records. MAT: Lake Tana (Loomis et al., 2015), Garba Guracha (this study), $\delta^{18}\text{O}_{\text{lake water}}$ as reconstructed from the aquatic sugar biomarker fucose (Bittner et al., 2021), Lake Turkana (Berke et al., 2012b; Morrissey et al., 2018), Lake Mahoma (Garelick et al., 2022), Sacred Lake (Loomis et al., 2012), Lake Rutundu (Loomis et al., 2017), Lake Victoria (Berke et al., 2012a), eastern Africa temperature stack (Ivory and Russell, 2018), and insolation 6°N and June 20°N (Laskar et al., 2004).

Lake Rutundu, and the Congo Basin by Ivory and Russell (2018) showed the highest temperatures between ~ 7 and ~ 4.5 ka cal BP. The timing of the highest reconstructed temperatures at these sites is not related to greenhouse gas radiative forcing or insolation forcing (Loomis et al., 2015). Loomis et al. (2015) point out that the Lake Tana and Sacred Lake temperature maxima lag Northern Hemisphere summer insolation, and Lake Malawi and Lake Tanganyika lead peak southern summer insolation. In the case of Garba Guracha, the highest temperatures coincide with local maximum September insolation at the site latitude of 6° N (Laskar et al., 2004) (Fig. 8). This matches the suggestion of Berke et al. (2012b) that the thermal optimum of several eastern African lakes might be determined by local solar irradiance from September to December (maximum at ~ 6 ka cal BP) (Fig. 8) rather than Northern Hemisphere summer solar irradiance. The restratification processes of eastern African lakes in these months and associated epilimnetic heating might explain the increased warming of lake water (Berke et al., 2012b). However, modelling studies do not support this hypothesis (Dee et al., 2021).

In addition to local insolation changes, local changes in P/E could have the potential to modify the lake water temperature. During the Early Holocene and Mid-Holocene, reconstructed high temperatures occurred during the African Humid Period, accompanied by the wettest phase of Garba Guracha (Bittner et al., 2021) and rising lake levels in the region (Gasse, 2000; Junginger et al., 2014), indicating higher amounts of precipitation due to an intensification of the monsoon system. A modelling study (Tierney et al., 2011a) proposes that during the AHP, the precipitation increase occurred mainly in June, July, and August (JJA), shortening the duration of annual drought phases in eastern Africa. Increased relative humidity would reduce evaporation, limiting the evaporative cooling of the lake water. Less evaporation, due to either shorter drought phases or generally higher precipitation, would increase the temperature and cause less positive $\delta^{18}\text{O}_{\text{lake water}}$ values, as suggested for Garba Guracha (Bittner et al., 2021).

The highest temperatures of the Holocene continued until 5.8 ka cal BP, interrupted only by a short drop in temperature after 7 ka cal BP. This is in agreement with the Sacred Lake temperature record (Loomis et al., 2012). Lake Tana experienced a shift towards colder conditions a bit earlier, from 7.5 to 7 ka cal BP (Loomis et al., 2015).

5.3.3 Cooling in the Late Holocene

After 5.8 ka cal BP, the MAT continuously decreased by $\sim 3.6^\circ\text{C}$ until recent times, coinciding with the summer insolation decline and decreasing temperatures of equatorial lakes (Ivory and Russell, 2018), Lake Tana (Loomis et al., 2015) and the marine Gulf of Aden record (Tierney et al., 2016). The general decreasing temperature trend is also supported by $\delta^{18}\text{O}_{\text{lake water}}$, pollen, and charcoal results showing

a decrease in moisture availability and fire activity at Garba Guracha (Bittner et al., 2021; Gil-Romera et al., 2019). Furthermore, an upward shift of the lower and dry forests during this time reinforces the idea of more intense evapotranspiration due to the decrease in moisture availability (Gil-Romera et al., 2021). A drop in TOC and decreasing $\delta^{13}\text{C}$ values (Bittner et al., 2020) support overall shifting catchment conditions.

During the last 2000 years, we observed that the increasing temperature trend concurred with an abrupt increase in the main woody communities and enhanced fire activities around Garba Guracha (Gil-Romera et al., 2021). However, we cannot discard human influence favouring both woody encroachment and fire activity.

The strong connection of temperature, P/E , and insolation across the Holocene shows that the Garba Guracha temperatures might have been affected by local radiation, possibly in interplay with insolation-driven atmospheric circulation changes and their impacts on air mass source, cloud cover, and evaporation. As current global warming continues, the intense warming of landmasses could lead to a major and complex restructuring of the atmospheric circulation system in the future, affecting eastern Africa and possibly even larger regions beyond via teleconnections.

6 Conclusions

Eastern African climatic history is spatially very diverse, and the driving mechanisms are complex and not fully understood. In eastern Africa, temperature reconstructions are generally sparse, especially in the high altitudes of the Horn of Africa. In this study, we used brGDGT from a high-altitude sedimentary record of the Bale Mountains (lake Garba Guracha, southwestern Ethiopia) to produce the first temperature reconstruction for the Horn of Africa.

The composition of brGDGT isomers in sediment records is affected by several influences, mainly by MAT, but in addition by lake water chemistry (pH and conductivity) and bacterial community, resulting in locally unique brGDGT compositions. For instance, in some of the Bale Mountains lakes, the abundance of a specific isomer IIIa' is uncommonly high in surface sediments. However, the summed abundance of IIIa and IIIa' is similar to other comparable lake archives in eastern Africa. We suspect that in the case of the Bale Mountains, changes in the lakes' water chemistry (pH and conductivity) or bacterial community are responsible for the high production of IIIa' at the expense of IIIa under drier conditions. By including the 6-methyl isomer in a temperature calibration, we were able to enhance the correlation with MAT. Therefore, we conclude that 6-methyl isomers have an impact on temperature reconstructions, highlighting their inclusion in a Bale Mountains-specific temperature calibration. Using surface sediment data from Bale Mountains lakes and

the East African lake database, the best-performing temperature calibration is a modified MBT_{5ME}' including IIIa'.

With the use of the new calibration, the Garba Guracha MAT record reflects insolation variability as one of the main climatic drivers at millennial scales. Additional factors such as glacier and permafrost melting during deglaciation and the regional atmospheric circulation likely play a prominent role on shorter timescales. These additional mechanisms partly explain the asynchronicity between the Garba Guracha MAT record in the high-altitude Afroalpine region of the Horn of Africa and other eastern African lake records.

Further research is necessary to understand the influences on and the origin of brGDGT-producing communities, especially at high altitudes.

Code availability. The code related to this article is available online under <https://doi.org/10.5281/zenodo.7233768> (Bittner, 2022a).

Data availability. The data related to this article are available online under <https://doi.org/10.5281/zenodo.7233983> (Bittner, 2022b).

Supplement. The supplement related to this article is available online at: <https://doi.org/10.5194/bg-19-5357-2022-supplement>.

Author contributions. LB, GGR, HFL, and MZ collected the samples. LB, CDJ, JMR, and MZ developed the concept. LB and CDJ extracted, analysed, and interpreted the brGDGT data. LB led the manuscript writing with contributions and feedback from all authors. MZ acquired the funding and supervised the work.

Competing interests. The contact author has declared that none of the authors has any competing interests.

Disclaimer. Publisher's note: Copernicus Publications remains neutral with regard to jurisdictional claims in published maps and institutional affiliations.

Acknowledgements. This research was funded by the German Research Council (DFG, ZE 844/10–1) in the framework of the joint Ethio-European DFG Research Unit 2358 “The Mountain Exile Hypothesis: How humans benefited from and re-shaped African high altitude ecosystems during Quaternary climate changes”. We are grateful to the project coordination; the Philipps University of Marburg; Addis Ababa University; the Frankfurt Zoological Society; the Ethiopian Wolf Project; the Bale Mountains National Park; and the related staff members, especially Katinka Thielsen and Mekbib Fekadu, for their logistic assistance during our fieldwork. We thank the Ethiopian Wildlife Conservation Authority for permitting our research in the Bale Mountains National Park.

Financial support. This research has been supported by the Deutsche Forschungsgemeinschaft (grant no. ZE 844/10–1).

This open access publication was financed by the Saxon State and University Library Dresden (SLUB Dresden).

Review statement. This paper was edited by Sebastian Naeher and reviewed by Jonathan Raberg and one anonymous referee.

References

- Alley, R. B.: The Younger Dryas cold interval as viewed from central Greenland, *Quaternary Sci. Rev.*, 19, 213–226, [https://doi.org/10.1016/S0277-3791\(99\)00062-1](https://doi.org/10.1016/S0277-3791(99)00062-1), 2000.
- Baxter, A. J., Hopmans, E. C., Russell, J. M., and Sinninghe Damsté, J. S.: Bacterial GMGTs in East African lake sediments: Their potential as palaeotemperature indicators, *Geochim. Cosmochim. Ac.*, 259, 155–169, <https://doi.org/10.1016/j.gca.2019.05.039>, 2019.
- Berke, M. A., Johnson, T. C., Werne, J. P., Grice, K., Schouten, S., and Sinninghe Damsté, J. S.: Molecular records of climate variability and vegetation response since the Late Pleistocene in the Lake Victoria basin, East Africa, *Quaternary Sci. Rev.*, 55, 59–74, <https://doi.org/10.1016/j.quascirev.2012.08.014>, 2012a.
- Berke, M. A., Johnson, T. C., Werne, J. P., Schouten, S., and Sinninghe Damsté, J. S.: A mid-Holocene thermal maximum at the end of the African Humid Period, *Earth Planet. Sc. Lett.*, 351–352, 95–104, <https://doi.org/10.1016/j.epsl.2012.07.008>, 2012b.
- Bini, M., Zanchetta, G., Perşoiu, A., Cartier, R., Català, A., Cacho, I., Dean, J. R., Di Rita, F., Drysdale, R. N., Finnè, M., Isola, I., Jalali, B., Lirer, F., Magri, D., Masi, A., Marks, L., Mercuri, A. M., Peyron, O., Sadori, L., Sicre, M.-A., Welc, F., Zielhofer, C., and Brisset, E.: The 4.2 ka BP Event in the Mediterranean region: an overview, *Clim. Past*, 15, 555–577, <https://doi.org/10.5194/cp-15-555-2019>, 2019.
- Bittner, L.: PCA_code, Zenodo [code], <https://doi.org/10.5281/zenodo.7233768>, 2022a.
- Bittner, L.: Data_Bittner et al., 2022, Zenodo [data set], <https://doi.org/10.5281/zenodo.7233983>, 2022b.
- Bittner, L., Bliedner, M., Grady, D., Gil-Romera, G., Martin-Jones, C., Lemma, B., Mekonnen, B., Lamb, H. F., Yang, H., Glaser, B., Szidat, S., Salazar, G., Rose, N. L., Opgenoorth, L., Miehe, G., Zech, W., and Zech, M.: Revisiting afro-alpine Lake Garba Guracha in the Bale Mountains of Ethiopia: rationale, chronology, geochemistry, and paleoenvironmental implications, *J. Paleolimnol.*, 64, 293–314, <https://doi.org/10.1007/s10933-020-00138-w>, 2020.
- Bittner, L., Gil-Romera, G., Grady, D., Lamb, H. F., Lorenz, E., Weiner, M., Meyer, H., Bromm, T., Glaser, B., and Zech, M.: The Holocene lake-evaporation history of the afro-alpine Lake Garba Guracha in the Bale Mountains, Ethiopia, based on $\delta^{18}\text{O}$ records of sugar biomarker and diatoms, *Quaternary Res.*, 105, 1–14, <https://doi.org/10.1017/qua.2021.26>, 2021.
- Blom, R. G., Farr, T. G., Feynmann, J., Ruzmaikin, A., and Pailou, P.: The green Sahara: Climate change, hydrologic history and human occupation, *IEEE Rad. Conf.*, 2009, 1–4, <https://doi.org/10.1109/RADAR.2009.4977129>, 2009.

- Bonnefille, R., Chalié, F., Guiot, J., and Vincens, A.: Quantitative estimates of full glacial temperatures in equatorial Africa from palynological data*, *Clim. Dynam.*, 6, 251–257, <https://doi.org/10.1007/BF00193538>, 1992.
- Castañeda, I. S., Schouten, S., Pätzold, J., Lucassen, F., Kasemann, S., Kuhlmann, H., and Schefuß, E.: Hydroclimate variability in the Nile River Basin during the past 28 000 years, *Earth Planet. Sc. Lett.*, 438, 47–56, <https://doi.org/10.1016/j.epsl.2015.12.014>, 2016.
- Cheddadi, R., Lamb, H. F., Guiot, J., and van der Kaars, S.: Holocene climatic change in Morocco: a quantitative reconstruction from pollen data, *Clim. Dynam.*, 14, 883–890, <https://doi.org/10.1007/s003820050262>, 1998.
- Chevalier, M. and Chase, B. M.: Southeast African records reveal a coherent shift from high- to low-latitude forcing mechanisms along the east African margin across last glacial–interglacial transition, *Quaternary Sci. Rev.*, 125, 117–130, <https://doi.org/10.1016/j.quascirev.2015.07.009>, 2015.
- Costa, K., Russell, J., Konecky, B., and Lamb, H.: Isotopic reconstruction of the African Humid Period and Congo Air Boundary migration at Lake Tana, Ethiopia, *Quaternary Sci. Rev.*, 83, 58–67, <https://doi.org/10.1016/j.quascirev.2013.10.031>, 2014.
- Damsté, J. S. S., Hopmans, E. C., Pancost, R. D., Schouten, S., and Geenevasen, J. A. J.: Newly discovered non-isoprenoid glycerol dialkyl glycerol tetraether lipids in sediments, *Chem. Commun.*, 2000, 1683–1684, <https://doi.org/10.1039/b004517i>, 2000.
- De Jonge, C., Hopmans, E. C., Zell, C. I., Kim, J.-H., Schouten, S., and Sinninghe Damsté, J. S.: Occurrence and abundance of 6-methyl branched glycerol dialkyl glycerol tetraethers in soils: Implications for palaeoclimate reconstruction, *Geochim. Cosmochim. Ac.*, 141, 97–112, <https://doi.org/10.1016/j.gca.2014.06.013>, 2014.
- De Jonge, C., Radujković, D., Sigurdsson, B. D., Weedon, J. T., Janssens, I., and Peterse, F.: Lipid biomarker temperature proxy responds to abrupt shift in the bacterial community composition in geothermally heated soils, *Org. Geochem.*, 137, 103897, <https://doi.org/10.1016/j.orggeochem.2019.07.006>, 2019.
- De Jonge, C., Kuramae, E. E., Radujković, D., Weedon, J. T., Janssens, I. A., and Peterse, F.: The influence of soil chemistry on branched tetraether lipids in mid- and high latitude soils: Implications for brGDGT-based paleothermometry, *Geochim. Cosmochim. Ac.*, 310, 95–112, <https://doi.org/10.1016/j.gca.2021.06.037>, 2021.
- Dearing Crampton-Flood, E., Tierney, J. E., Peterse, F., Kirkels, F. M. S. A., and Sinninghe Damsté, J. S.: BayMBT: A Bayesian calibration model for branched glycerol dialkyl glycerol tetraethers in soils and peats, *Geochim. Cosmochim. Ac.*, 268, 142–159, <https://doi.org/10.1016/j.gca.2019.09.043>, 2020.
- Dee, S. G., Morrill, C., Kim, S. H., and Russell, J. M.: Hot Air, Hot Lakes, or Both? Exploring Mid-Holocene African Temperatures Using Proxy System Modeling, *J. Geophys. Res.-Atmos.*, 126, e2020JD033269, <https://doi.org/10.1029/2020JD033269>, 2021.
- deMenocal, P., Ortiz, J., Guilderson, T., Adkins, J., Sarnthein, M., Baker, L., and Yarusinsky, M.: Abrupt onset and termination of the African Humid Period., *Quaternary Sci. Rev.*, 19, 347–361, [https://doi.org/10.1016/S0277-3791\(99\)00081-5](https://doi.org/10.1016/S0277-3791(99)00081-5), 2000.
- Eggermont, H., Wondafraash, M., Van Damme, M., Lens, K., and Umer M. H.: Bale Moluntains Lakes: Ecosystems under pressure of global change?, *Walia*, 2011, 171–180, https://hdl.handle.net/10520/AJA00837059_148 (last access: 24 October 2022), 2011.
- Eggermont, H., Heiri, O., James, A., Ae, R., Vuille, M., Leen, A., Ae, A., and Verschuren, D.: Paleotemperature reconstruction in tropical Africa using fossil Chironomidae (Insecta: Diptera), *J. Paleolimnol.*, 43, 413–435, <https://doi.org/10.1007/s10933-009-9339-2>, 2010.
- Garellick, S., Russell, J. M., Dee, S., Verschuren, D., and Olago, D. O.: Atmospheric controls on precipitation isotopes and hydroclimate in high-elevation regions in Eastern Africa since the Last Glacial Maximum, *Earth Planet. Sc. Lett.*, 567, 116984, <https://doi.org/10.1016/j.epsl.2021.116984>, 2021.
- Garellick, S., Russell, J., Richards, A., Smith, J., Kelly, M., Anderson, N., Jackson, M. S., Doughty, A., Nakileza, B., Ivory, S., Dee, S., and Marshall, C.: The dynamics of warming during the last deglaciation in high-elevation regions of Eastern Equatorial Africa, *Quaternary Sci. Rev.*, 281, 107416, <https://doi.org/10.1016/j.quascirev.2022.107416>, 2022.
- Gasse, F.: Hydrological changes in the African tropics since the Last Glacial Maximum, *Quaternary Sci. Rev.*, 19, 189–211, [https://doi.org/10.1016/S0277-3791\(99\)00061-X](https://doi.org/10.1016/S0277-3791(99)00061-X), 2000.
- Gil-Romera, G., Adolf, C., Benito Blas, M., Bittner, L., Johansson, M. M. U., Grady, D. D. A., Lamb, H. H. F., Lemma, B., Fekadu, M., Glaser, B., Mekonnen, B., Sevilla-Callejo, M., Zech, M., Zech, W., and Mieke, G.: Long-term fire resilience of the Ericaean Belt, Bale Mountains, Ethiopia, *Biol. Lett.-UK*, 15, 20190357, <https://doi.org/10.1098/rsbl.2019.0357>, 2019.
- Gil-Romera, G., Fekadu, M., Opgenoorth, L., Grady, D., Lamb, H. F., Bittner, L., Zech, M., and Mieke, G.: The new Garba Guracha palynological sequence: Revision and data expansion, in: *Quaternary Vegetation Dynamics – The African Pollen Database*, edited by: Runge, J., Gosling, W. D., Lézine, A.-M., and Scott, L., CRC Press, London, 442, <https://doi.org/10.1201/9781003162766>, 2021.
- Groos, A. R., Akçar, N., Yesilyurt, S., Mieke, G., Vockenhuber, C., and Veit, H.: Nonuniform Late Pleistocene glacier fluctuations in tropical Eastern Africa, *Science Advances*, 7, eabb6826, <https://doi.org/10.1126/sciadv.abb6826>, 2021a.
- Groos, A. R., Niederhauser, J., Wraase, L., Hänsel, F., Naus, T., Akçar, N., and Veit, H.: The enigma of relict large sorted stone stripes in the tropical Ethiopian Highlands, *Earth Surf. Dynam.*, 9, 145–166, <https://doi.org/10.5194/esurf-9-145-2021>, 2021b.
- Halamka, T. A., McFarlin, J. M., Younkun, A. D., Depoy, J., Dildar, N., and Kopf, S. H.: Oxygen limitation can trigger the production of branched GDGTs in culture, *Geochemical Perspectives Letters*, 19, 36–39, 2021.
- Hillman, J.: *The Bale Mountains National Park Area, Southeast Ethiopia, and Its Management*, Mountain Research and Development, 253 pp., <https://doi.org/10.2307/3673456>, 1988.
- Hopmans, E. C., Weijers, J. W. H., Schefuß, E., Herfort, L., Sinninghe Damsté, J. S., and Schouten, S.: A novel proxy for terrestrial organic matter in sediments based on branched and isoprenoid tetraether lipids, *Earth Planet. Sc. Lett.*, 224, 107–116, <https://doi.org/10.1016/j.epsl.2004.05.012>, 2004.
- Hopmans, E. C., Schouten, S., and Sinninghe Damsté, J. S.: The effect of improved chromatography on GDGT-based palaeoproxies, *Org. Geochem.*, 93, 1–6, <https://doi.org/10.1016/j.orggeochem.2015.12.006>, 2016.

- Hove, H., Echeverria, D., and Parry, J.-E.: Review of current and planned adaptation action: East Africa, International Institute for Sustainable Development, Winnipeg, 2011.
- Hughes, A. C., Orr, M. C., Ma, K., Costello, M. J., Waller, J., Provoost, P., Yang, Q., Zhu, C., and Qiao, H.: Sampling biases shape our view of the natural world, *Ecography*, 44, 1259–1269, <https://doi.org/10.1111/ecog.05926>, 2021.
- Huguet, C., Kim, J. H., Damsté, J. S. S., and Schouten, S.: Reconstruction of sea surface temperature variations in the Arabian Sea over the last 23 kyr using organic proxies (TEX₈₆ and U_{37K'}), *Paleoceanography*, 21, PA3003, <https://doi.org/10.1029/2005PA001215>, 2006.
- Huybers, P.: Early Pleistocene Glacial Cycles and the Integrated Summer Insolation Forcing, *Science*, 313, 508–511, <https://doi.org/10.1126/science.1125249>, 2006.
- IPCC: Climate Change 2021: The Physical Science Basis. Contribution of Working Group I to the Sixth Assessment Report of the Intergovernmental Panel on Climate Change, edited by: Masson-Delmotte, V., Zhai, P., Pirani, A., Connors, S. L., Péan, C., Berger, S., Caud, N., and Chen, Y., Cambridge University Press, 2021.
- Ivory, S. J. and Russell, J.: Lowland forest collapse and early human impacts at the end of the African Humid Period at Lake Edward, equatorial East Africa, *Quaternary Res.*, 89, 7–20, <https://doi.org/10.1017/qua.2017.48>, 2018.
- Jaeschke, A., Thienemann, M., Schefuß, E., Urban, J., Schäbitz, F., Wagner, B., and Rethemeyer, J.: Holocene Hydroclimate Variability and Vegetation Response in the Ethiopian Highlands (Lake Dendi), *Front. Earth Sci.*, 8, 1–14, <https://doi.org/10.3389/feart.2020.585770>, 2020.
- Junginger, A., Roller, S., Olaka, L. A., and Trauth, M. H.: The effects of solar irradiation changes on the migration of the Congo Air Boundary and water levels of paleo-Lake Suguta, Northern Kenya Rift, during the African Humid Period (15–5 ka BP), *Palaeogeogr. Palaeoclimatol.*, 396, 1–16, <https://doi.org/10.1016/j.palaeo.2013.12.007>, 2014.
- Kassambara, A. and Mundt, F.: factoextra: Extract and Visualise the Results of Multivariate Data Analyses, <https://cran.r-project.org/package=factoextra> (last access: 1 April 2022), 2020.
- Kidane, Y., Stahlmann, R., and Beierkuhnlein, C.: Vegetation dynamics, and land use and land cover change in the Bale Mountains, Ethiopia, *Environ. Monit. Assess.*, 184, 7473–7489, <https://doi.org/10.1007/s10661-011-2514-8>, 2012.
- Laskar, J., Robutel, P., Joutel, F., Gastineau, M., Correia, A. C. M., and Levrard, B.: A long-term numerical solution for the insolation quantities of the Earth, *A&A*, 428, 261–285, 2004.
- Löffler, H.: Limnology and paleolimnological data on the Bale Mountain Lakes, Verth, International Verein. *Limnology*, 20, 1131–1138, 1978.
- Loomis, S. E., Russell, J. M., and Sinninghe Damsté, J. S.: Distributions of branched GDGTs in soils and lake sediments from western Uganda: Implications for a lacustrine paleothermometer, *Org. Geochem.*, 42, 739–751, <https://doi.org/10.1016/j.orggeochem.2011.06.004>, 2011.
- Loomis, S. E., Russell, J. M., Ladd, B., Street-Perrott, F. A., and Sinninghe Damsté, J. S.: Calibration and application of the branched GDGT temperature proxy on East African lake sediments, *Earth Planet. Sc. Lett.*, 357–358, 277–288, <https://doi.org/10.1016/j.epsl.2012.09.031>, 2012.
- Loomis, S. E., Russell, J. M., Heurreux, A. M., D'Andrea, W. J., and Sinninghe Damsté, J. S.: Seasonal variability of branched glycerol dialkyl glycerol tetraethers (brGDGTs) in a temperate lake system, *Geochim. Cosmochim. Ac.*, 144, 173–187, <https://doi.org/10.1016/j.gca.2014.08.027>, 2014.
- Loomis, S. E., Russell, J. M., and Lamb, H. F.: North-east African temperature variability since the Late Pleistocene, *Palaeogeogr. Palaeoclimatol.*, 423, 80–90, <https://doi.org/10.1016/j.palaeo.2015.02.005>, 2015.
- Loomis, S. E., Russell, J. M., Verschuren, D., Morrill, C., De Cort, G., Sinninghe Damsté, J. S., Olago, D., Eggermont, H., Street-Perrott, F. A., and Kelly, M. A.: The tropical lapse rate steepened during the Last Glacial Maximum, *Science Advances*, 3, e1600815, <https://doi.org/10.1126/sciadv.1600815>, 2017.
- Lyon, B. and Vigaud, N.: Unraveling East Africa's Climate Paradox, <https://doi.org/10.1002/9781119068020.ch16>, 2017.
- Marshall, M., Lamb, H., Davies, S., Leng, M., Bedaso, Z., Umer, M., and Bryant, C.: Climatic change in northern Ethiopia during the past 17 000 years: A diatom and stable isotope record from Lake Ashenge, *Palaeogeogr. Palaeoclimatol.*, 279, 114–127, <https://doi.org/10.1016/j.palaeo.2009.05.003>, 2009.
- Martínez-Sosa, P., Tierney, J. E., Stefanescu, I. C., Crampton-Flood, E. D., Shuman, B. N., and Routson, C.: A global Bayesian temperature calibration for lacustrine brGDGTs, <https://doi.org/10.1594/PANGAEA.931169>, last access: 6 May 2021.
- Miehe, S. and Miehe, G.: Ericaceous forests and heathlands in the Bale mountains of South Ethiopia, Hamburg, Warnke, ISBN 9783980159142, 1994.
- Morrissey, A. and Scholz, C. A.: Paleohydrology of Lake Turkana and its influence on the Nile River system, *Palaeogeogr. Palaeoclimatol.*, 403, 88–100, <https://doi.org/10.1016/j.palaeo.2014.03.029>, 2014.
- Morrissey, A., Scholz, C. A., and Russell, J. M.: Late Quaternary TEX₈₆ paleotemperatures from the world's largest desert lake, Lake Turkana, Kenya, *J. Paleolimnol.*, 59, 103–117, <https://doi.org/10.1007/s10933-016-9939-6>, 2018.
- Neukom, R., Barboza, L. A., Erb, M. P., Shi, F., Emile-Geay, J., Evans, M. N., Franke, J., Kaufman, D. S., Lücke, L., Rehfeld, K., Schurer, A., Zhu, F., Brönnimann, S., Hakim, G. J., Henley, B. J., Ljungqvist, F. C., McKay, N., Valler, V., and von Gunten, L.: Consistent multidecadal variability in global temperature reconstructions and simulations over the Common Era, *Nat. Geosci.*, 12, 643–649, <https://doi.org/10.1038/s41561-019-0400-0>, 2019.
- Nicholson, S. E.: Climate and climatic variability of rainfall over eastern Africa, *Rev. Geophys.*, 55, 590–635, <https://doi.org/10.1002/2016RG000544>, 2017.
- Osmaston, H. A., Mitchell, W. A., and Osmaston, J. A. N.: Quaternary glaciation of the Bale Mountains, Ethiopia, *J. Quaternary Sci.*, 20, 593–606, <https://doi.org/10.1002/jqs.931>, 2005.
- Ossendorf, G., Groos, A., Bromm, T., Girma Tekelemariam, M., Glaser, B., Lesur, J., Schmidt, J., Akçar, N., Bekele, T., Beldados, A., Demissew, S., Hadush Kahsay, T., Nash, B. P., Naus, T., Negash, A., Nemomissa, S., Veit, H., Vogelsang, R., Zerihun, W., and Miehe, G.: Middle Stone Age foragers resided in high elevations of the glaciated Bale Mountains, Ethiopia, *Science*, 365, 583–587, 2019.
- Otto-Bliesner, B. L., Russell, J. M., Clark, P. U., Liu, Z., Overpeck, J. T., Konecky, B., DeMenocal, P., Nicholson, S. E., He, F., and

- Lu, Z.: Coherent changes of south-eastern equatorial and northern African rainfall during the last deglaciation, *Science*, 346, 1223–1227, <https://doi.org/10.1126/science.1259531>, 2014.
- Peterse, F., van der Meer, J., Schouten, S., Weijers, J. W. H., Fierer, N., Jackson, R. B., Kim, J.-H., and Sinninghe Damsté, J. S.: Revised calibration of the MBT–CBT paleotemperature proxy based on branched tetraether membrane lipids in surface soils, *Geochim. Cosmochim. Ac.*, 96, 215–229, <https://doi.org/10.1016/j.gca.2012.08.011>, 2012.
- Powers, L. A., Johnson, T. C., Werne, J. P., Castañeda, I. S., Hopmans, E. C., Sinninghe Damsté, J. S., and Schouten, S.: Large temperature variability in the southern African tropics since the Last Glacial Maximum, *Geophys. Res. Lett.*, 32, 1–4, <https://doi.org/10.1029/2004GL022014>, 2005.
- R Core Team: R: A Language and Environment for Statistical Computing, <https://www.r-project.org/> (last access: 1 April 2022), 2021.
- Raberg, J. H., Harning, D. J., Crump, S. E., de Wet, G., Blumm, A., Kopf, S., Geirsdóttir, Á., Miller, G. H., and Sepúlveda, J.: Revised fractional abundances and warm-season temperatures substantially improve brGDGT calibrations in lake sediments, *Biogeosciences*, 18, 3579–3603, <https://doi.org/10.5194/bg-18-3579-2021>, 2021.
- Russell, J. M., Hopmans, E. C., Loomis, S. E., Liang, J., and Sinninghe Damsté, J. S.: Distributions of 5- and 6-methyl branched glycerol dialkyl glycerol tetraethers (brGDGTs) in East African lake sediment: Effects of temperature, pH, and new lacustrine paleotemperature calibrations, *Org. Geochem.*, 117, 56–69, <https://doi.org/10.1016/j.orggeochem.2017.12.003>, 2018.
- Schouten, S., Forster, A., Panoto, F. E., and Sinninghe Damsté, J. S.: Towards calibration of the TEX₈₆ palaeothermometer for tropical sea surface temperatures in ancient greenhouse worlds, *Org. Geochem.*, 38, 1537–1546, <https://doi.org/10.1016/j.orggeochem.2007.05.014>, 2007.
- Schreuder, L. T., Beets, C. J., Prins, M. A., Hatté, C., and Peterse, F.: Late Pleistocene climate evolution in South-eastern Europe recorded by soil bacterial membrane lipids in Serbian loess, *Palaeogeogr. Palaeoclimatol.*, 449, 141–148, <https://doi.org/10.1016/j.palaeo.2016.02.013>, 2016.
- Sinninghe Damsté, J. S., Rijpstra, W. I. C., Foesel, B. U., Huber, K. J., Overmann, J., Nakagawa, S., Kim, J. J., Dunfield, P. F., Dedysh, S. N., and Villanueva, L.: An overview of the occurrence of ether- and ester-linked iso-diabolic acid membrane lipids in microbial cultures of the Acidobacteria: Implications for brGDGT paleoproxies for temperature and pH, *Org. Geochem.*, 124, 63–76, <https://doi.org/10.1016/j.orggeochem.2018.07.006>, 2018.
- Thompson, R. S.: The role of paleoclimatic studies in assessing climate change, *EOS*, 85, 436, <https://doi.org/10.1029/2004EO430005>, 2004.
- Tiercelin, J. J., Gibert, E., Umer, M., Bonnefille, R., Disnar, J. R., Lézine, A. M., Hureau-Mazaudier, D., Travi, Y., Keravis, D., and Lamb, H. F.: High-resolution sedimentary record of the last deglaciation from a high-altitude lake in Ethiopia, *Quaternary Sci. Rev.*, 27, 449–467, <https://doi.org/10.1016/j.quascirev.2007.11.002>, 2008.
- Tierney, J. E. and deMenocal, P. B.: Abrupt Shifts in Horn of Africa Hydroclimate Since the Last Glacial Maximum, *Science*, 342, 843–846, <https://doi.org/10.1126/science.1240411>, 2013.
- Tierney, J. E. and Russell, J. M.: Abrupt climate change in south-east tropical Africa influenced by Indian monsoon variability and ITCZ migration, *Geophys. Res. Lett.*, 34, L15709, <https://doi.org/10.1029/2007GL029508>, 2007.
- Tierney, J. E., Russell, J. M., Huang, Y., Damsté, J. S. S., Hopmans, E. C., and Cohen, A. S.: Northern Hemisphere Controls on Tropical Southeast African Climate During the Past 60000 Years, *Science*, 322, 252–255, <https://doi.org/10.1126/science.1160485>, 2008.
- Tierney, J. E., Lewis, S. C., Cook, B. I., LeGrande, A. N., and Schmidt, G. A.: Model, proxy and isotopic perspectives on the East African Humid Period, *Earth Planet. Sc. Lett.*, 307, 103–112, <https://doi.org/10.1016/j.epsl.2011.04.038>, 2011a.
- Tierney, J. E., Russell, J. M., Sinninghe Damsté, J. S., Huang, Y., and Verschuren, D.: Late Quaternary behavior of the East African monsoon and the importance of the Congo Air Boundary, *Quaternary Sci. Rev.*, 30, 798–807, <https://doi.org/10.1016/j.quascirev.2011.01.017>, 2011b.
- Tierney, J. E., Smerdon, J. E., Anchukaitis, K. J., and Seager, R.: Multidecadal variability in East African hydroclimate controlled by the Indian Ocean, *Nature*, 493, 389–392, <https://doi.org/10.1038/nature11785>, 2013.
- Tierney, J. E., Pausata, F. S. R., and Demenocal, P.: Deglacial Indian monsoon failure and North Atlantic stadials linked by Indian Ocean surface cooling, *Nat. Geosci.*, 9, 46–50, <https://doi.org/10.1038/ngeo2603>, 2016.
- Tierney, J. E., Pausata, F. S. R., and DeMenocal, P. B.: Rainfall regimes of the Green Sahara, *Science Advances*, 3, e1601503, <https://doi.org/10.1126/sciadv.1601503>, 2017.
- Trauth, M. H., Foerster, V., Junginger, A., Asrat, A., Lamb, H. F., and Schaebitz, F.: Abrupt or gradual? Change point analysis of the late Pleistocene–Holocene climate record from Chew Bahir, southern Ethiopia, *Quaternary Res.*, 90, 321–330, <https://doi.org/10.1017/qua.2018.30>, 2018.
- Uhlir, S. and Uhlir, K.: Studies on the Altitudinal Zonation of Forests and Alpine Plants in the Central Bale Mountains, Ethiopia, 153 pp., <https://doi.org/10.2307/3673574>, 1991.
- Uhlir, S. K.: Mountain Forests and the Upper Tree Limit on the Southeastern Plateau of Ethiopia, *Mt. Res. Dev.*, 8, 227–234, <https://doi.org/10.2307/3673452>, 1988.
- Umer, M., Lamb, H. F., Bonnefille, R., Lézine, A. M., Tiercelin, J. J., Gibert, E., Cazet, J. P., and Watrin, J.: Late Pleistocene and Holocene vegetation history of the Bale Mountains, Ethiopia, *Quaternary Sci. Rev.*, 26, 2229–2246, <https://doi.org/10.1016/j.quascirev.2007.05.004>, 2007.
- van Bree, L. G. J., Peterse, F., Baxter, A. J., De Crop, W., van Grinsven, S., Villanueva, L., Verschuren, D., and Sinninghe Damsté, J. S.: Seasonal variability and sources of in situ brGDGT production in a permanently stratified African crater lake, *Biogeosciences*, 17, 5443–5463, <https://doi.org/10.5194/bg-17-5443-2020>, 2020.
- Wagner, B., Wennrich, V., Viehberg, F., Junginger, A., Kolvenbach, A., Rethemeyer, J., Schaebitz, F., and Schmiidl, G.: Holocene rainfall runoff in the central Ethiopian highlands and evolution of the River Nile drainage system as revealed from a sediment record from Lake Dendi, *Global Planet. Change*, 163, 29–43, <https://doi.org/10.1016/j.gloplacha.2018.02.003>, 2018.
- Wang, H., Liu, W., He, Y., Zhou, A., Zhao, H., Liu, H., Cao, Y., Hu, J., Meng, B., Jiang, J., Kolpakova, M., Krivono-

- gov, S., and Liu, Z.: Salinity-controlled isomerisation of lacustrine brGDGTs impacts the associated MBT5ME' terrestrial temperature index, *Geochim. Cosmochim. Ac.*, 305, 33–48, <https://doi.org/10.1016/j.gca.2021.05.004>, 2021.
- Weber, Y., Damsté, J. S. S., Zopfi, J., De Jonge, C., Gilli, A., Schubert, C. J., Lepori, F., Lehmann, M. F., and Niemann, H.: Redox-dependent niche differentiation provides evidence for multiple bacterial sources of glycerol tetraether lipids in lakes, *P. Natl. Acad. Sci. USA*, 115, 10926–10931, <https://doi.org/10.1073/pnas.1805186115>, 2018.
- Weijers, J. W. H., Schefuß, E., Schouten, S., and Damsté, J. S. S.: Coupled thermal and hydrological evolution of tropical Africa over the last deglaciation, *Science*, 315, 1701–1704, <https://doi.org/10.1126/science.1138131>, 2007a.
- Weijers, J. W. H., Schouten, S., van den Donker, J. C., Hopmans, E. C., and Sinninghe Damsté, J. S.: Environmental controls on bacterial tetraether membrane lipid distribution in soils, *Geochim. Cosmochim. Ac.*, 71, 703–713, <https://doi.org/10.1016/j.gca.2006.10.003>, 2007b.
- Werdecker, J.: Eine Durchquerung des Goba-Massivs in Südäthiopien, *Hermann von Wissmann-Festschrift*, Tübingen, 132–144, 1962.
- Williams, F. M.: *The Southeastern Highlands and the Ogaden*, edited by: Williams, F. M., Springer International Publishing, Cham, 153–170, https://doi.org/10.1007/978-3-319-02180-5_15, 2016.
- Woldu, Z., Feoli, E., and Nigatu, L.: Partitioning an elevation gradient of vegetation from south-eastern Ethiopia by probabilistic methods, *Plant Ecol.*, 81, 189–198, 1989.
- Wu, H., Guiot, J., Brewer, S., and Guo, Z.: Climatic changes in Eurasia and Africa at the last glacial maximum and mid-Holocene: reconstruction from pollen data using inverse vegetation modelling, *Clim. Dynam.*, 29, 211–229, <https://doi.org/10.1007/s00382-007-0231-3>, 2007.
- Zeng, F. and Yang, H.: Temperature changes reconstructed from branched GDGTs on the central Loess Plateau during the past 130–5 ka, *Quaternary Int.*, 503, 3–9, <https://doi.org/10.1016/j.quaint.2018.04.045>, 2019.